metals

MDPI

Article

Synthesis of Ti–Al Bimodal Powder for High Flowability Feedstock by Electrical Explosion of Wires

Marat Lerner [1,2], Alexander Pervikov [1,2], Elena Glazkova [2,*], Nikolay Rodkevich [2], Konstantin Suliz [2], Sergey Kazantsev [2], Nikita Toropkov [1,2] and Olga Bakina [2]

[1] National Research Tomsk State University, 634050 Tomsk, Russia; lerner@ispms.tsc.ru (M.L.); pervikov@list.ru (A.P.); zerogooff@gmail.com (N.T.)
[2] Institute of Strength Physics and Material Science, Siberian Branch of Russian Academy of Science, 634055 Tomsk, Russia; ngradk@ispms.tsc.ru (N.R.); konstantin.suliz@gmail.com (K.S.); kzso@ispms.tsc.ru (S.K.); ovbakina@ispms.tsc.ru (O.B.)
* Correspondence: eagl@ispms.tsc.ru

Abstract: In this research, Ti–Al bimodal powders were produced by simultaneous electrical explosion of titanium and aluminum wires. The resulting powders were used to prepare powder–polymer feedstocks. Material characterization involving X-ray diffraction (XRD), transmission electron microscopy (TEM), scanning electron microscopy (SEM), energy dispersive spectroscopy (EDS), and melt flow index (MFI) determination were carried out to characterize bimodal powders obtained and evaluate the influence of the powder composition on the feedstock flowability. The bimodal distribution of particles in powders has been found to be achieved at a current density of 1.2×10^7 A/cm^2 (the rate of energy input is 56.5 J/μs). An increase in the current density to 1.6×10^7 A/cm^2 leads to a decrease in the content of micron particles and turning into a monomodal particle size distribution. The use of bimodal powders for powder–polymer feedstocks allows to achieve higher MFI values compared with monomodal powders. In addition, the use of electroexplosive synthesis of bimodal powders makes it possible to achieve a homogeneous distribution of micro- and nanoparticles in the feedstock.

Keywords: electrical explosion; wire; energy; Ti–Al; bimodal powder; microparticles; nanoparticles; homogeneous; bimodal feedstock; flowability

check for updates

Citation: Lerner, M.; Pervikov, A.; Glazkova, E.; Rodkevich, N.; Suliz, K.; Kazantsev, S.; Toropkov, N.; Bakina, O. Synthesis of Ti–Al Bimodal Powder for High Flowability Feedstock by Electrical Explosion of Wires. *Metals* **2022**, *12*, 478. https://doi.org/10.3390/met12030478

Academic Editors: Ana Romero Gutiérrez and Ilaria Cristofolini

Received: 25 January 2022
Accepted: 8 March 2022
Published: 11 March 2022

Publisher's Note: MDPI stays neutral with regard to jurisdictional claims in published maps and institutional affiliations.

Copyright: © 2022 by the authors. Licensee MDPI, Basel, Switzerland. This article is an open access article distributed under the terms and conditions of the Creative Commons Attribution (CC BY) license (https://creativecommons.org/licenses/by/4.0/).

1. Introduction

Additive manufacturing (AM) technology for fabrication of complex shaped parts has many important applications in the automobile, aerospace and energy industries, biomedical applications and in other fields [1,2]. Fabrication of the parts by extrusion of thermoplastic polymer materials (FDM method) is a widespread method [3,4]. The possibility of AM of 3D objects using feedstocks considered as composite material comprising metal or ceramic micropowders and a polymer binder has been shown [5]. To reduce the viscosity of the feedstock, the use of binders such as wax or polyethylene glycol (PEG) was proposed [6,7].

To improve the performance of the parts fabricated, the promising solution is to incorporate nanoparticles into the feedstock formulation. The nanoparticles in the feedstock formulation are considered as an additional binder used in combination with a polymer binder. It was noted that the hardness of the sintered material increases as the fraction of nanoparticles in the feedstock increases [8].

However, a large specific surface area of nanopowders leads to strong agglomeration of nanoparticles and high interparticle friction, which reduces the packing density and can lead to an increase in the porosity of the bulk material [9]. Moreover, metal nanopowders are prone to spontaneous explosive oxidation and have a high cost, which limits their widespread use.

Considering the above, more promising components of the feedstock formulation are bimodal powders containing both micro- (particle size more than 1 μm) and nanosized (particle size less than 100 nm) particles of a given composition. For example, when using bimodal powders in powder metallurgy, the disadvantages of nanopowders are reduced, and their advantages are generally preserved [10]. Powder composites based on micro- and nanoparticles provide a higher density of the final part in various powder processing methods, since nanoparticles fill the gaps between microparticles [11–14]. For example, the addition of iron nanoparticles to micropowders has been reported to lead to 95% increase in the ultimate flexural strength of steel parts, and 60% decrease in sintering shrinkage [15].

The feedstock comprising bimodal powders, known as bimodal feedstock, allows increased powder bed packing density and a higher density of printed parts than that based on micropowders [16]. Such bimodal feedstocks can provide a new breakthrough in the development of optimal raw material formulations for injection molding at low temperatures and pressures as well as 3D printing. Furthermore, bimodal feedstock is characterized by reduced viscosity.

A composition of micro- and nanoparticles (25 vol.%) of 316 L stainless steel combined with a polymer binder (a mixture of paraffin, wax, and stearic acid) showed a pseudoplastic flow [8]. Feedstock included both nanoparticles (content in the material 20 vol.% and 30 vol.%) and microparticles of stainless steel 316 L and a binder (73 vol.% PEG, 25 vol.% polymethyl methacrylate, and 2 vol.% stearic acid) also showed pseudoplastic flow and had a lower viscosity than microparticulate feedstock [17].

Since there are many interfaces between two dispersed phases (micro- and nano-phases), the properties of the composite are determined by phase interactions at these interfaces. The distribution of micro- and nanosized particles in the powder composite should be uniform in order to ensure the same properties throughout the volume of the material. The regular distribution of nanoparticles in a bimodal powder plays a decisive role in the sintering process of the material [10,18–21].

There are two approaches to obtain bimodal powders—the formation of homogeneous mixtures during the synthesis of powders and the mixing of pre-prepared nano- and microparticles with each other. However, mixing of microparticles and nanoparticles with a size of less than 100 nm, especially metals differing in density, can be a serious challenge. Currently, nano- and micro-powders are mixed in predetermined proportions, for example, using Turbula mixers. Bimodal composites of 316 L stainless steel from microparticles with a size of 4 μm and nanoparticles with a size of 100 nm [10], and iron with a microparticle size of 3 μm and nanoparticles of 100 nm [19] with a Fe nanoparticle content of 25, 50, and 75 vol.% were prepared in this way. Deagglomeration of nanopowders and uniform mixing of nanoparticles with a size of 150 nm and microparticles with a size of 5 μm was carried out using a ball mill [17]. The advantage of the process of mixing pre-prepared nano- and microparticles is that it is possible to precisely control the ratio of dispersed phases in the composition. However, this method is still at the laboratory stage and does not allow obtaining homogeneous mixtures of nano- and microparticles in the number of tens of kilograms.

Methods that ensure the formation of uniform mixtures of nano- and microparticles during in situ preparation of powders may turn out to be more promising for the production of large amounts of bimodal composites. Thus, a method for preparing a bimodal mixture of nano- and micro-particles of copper with a polymer protective coating during reduction of copper salts has been proposed [22]. However, despite the high homogeneity of the mixture, it is difficult to precisely control the ratio of nano- and microparticles in the powder. In addition, the methods of chemical synthesis are not universal and make it possible to obtain only bimodal powders of one metal, although powders of alloys or several dissimilar metals are of greatest interest for practical application.

Thus, a powder composite consisting of spherically shaped tungsten microparticles coated with copper nanoparticles (5 wt.%) was obtained using inductively coupled thermal

plasma. The synthesized W–Cu composite powder showed a high packing density with a uniform distribution of W and Cu [23].

One of the promising methods for producing powders is the electrical explosion of wires (EEW). The electrical explosion occurs when a high-power current pulse with a density of 10^6–10^9 A/cm^2 flows through a metal wire, with the metal of the wire heated to the melting point, melted, and then explosively destroyed [24]. Depending on the kind of gas surrounding the wire and the metal exploded, the method of electrical explosion makes it possible to obtain nanopowders of metals, alloys, chemical compounds or composite nanopowders.

Sedoi [25] has established that to ensure a uniform heating of the wire by the current pulse over the wire and, consequently, the uniformity of the dispersed composition of the resulting nanopowders, the current density (j) and the wire diameter (d_0) shall meet the following conditions (1):

$$10^7 \text{ A/cm}^2 \leq j \leq 10^8 \text{ A/cm}^2; 0.1 \times 10^{-3} \text{ m} < d_0 \leq 0.5 \times 10^{-3} \text{ m} \quad (1)$$

These conditions make it possible to obtain metal nanoparticles with an average size of less than 100 nm [24], including for the development of bimodal composites for AM process. However, to obtain powder composites consisting of micro- and nanoparticles, different conditions for the electrical explosion of wires are required than those for the production of nanopowders. The dispersion process should allow, along with nanoparticles, to obtain microparticles.

In this work, the method for the synthesis of bimodal alloy powders by simultaneous electrical explosion of Ti and Al wires is discussed. The conditions for the electrical explosion of wires to obtain homogeneous mixtures of Ti–Al nano- and microparticles are investigated. The size, element distribution, and phase composition of the powders are evaluated as well. The bimodal powders prepared were used to develop powder–polymer feedstocks, i.e., bimodal feedstocks. The effect of disperse composition of the bimodal powders prepared on the bimodal feedstock flowability has been examined.

2. Materials and Methods

2.1. Preparation of Powders

Ti–Al bimodal powders were obtained by the EEW method using a setup reported previously [26–28]. Titanium and aluminum wires with a metal content of 99.9% were used in the experiments to obtain bimodal powders consisting of Ti–Al micro- and nanoparticles. The EEW process parameters are presented in Table 1, where C is the electric capacity of the capacitor bank, U_0 is the charging voltage of the capacitor bank. The energy $E(t)$ transferred to the wires and temporal characteristics of the EEW process for the titanium and aluminum wires were determined from corresponding time dependences of current $I(t)$ and voltage $U(t)$ recorded during the EEW process [26].

Table 1. The experimental parameters for the powder preparation.

Sample	U_0 (kV)	C (μF)	Wire Dimensions			
			Diameter (mm)		Length (mm)	
			Ti	Al	Ti	Al
1	15	1.6	0.31	0.25	70	70
2	21					
3	25					

The energy level transferred to the wires can be carried out by the voltage U_0 variation. The amount of energy transferred to wires is determined according to the expression (2) [27]:

$$E(t) = U_0 \int_0^t I(t)dt - \frac{1}{2C}[\int_0^t I(t)dt]^2 - \frac{LI^2(t)}{2} - R\int_0^t I^2(t)dt \quad (2)$$

where t—time of passage of the current pulse $I(t)$ through the wires, U_0 is the charging voltage of the capacitive energy storage, C is the total capacitance of the capacitive energy storage, L is the circuit intrinsic inductance, R is the circuit active resistance.

The first term on the right side of the Equation (2) is the energy transferred to the circuit; the second, third, and fourth ones are energy losses in the capacitive storage, on the inductance and active resistance of the circuit, respectively.

2.2. Characterization of Powders

The particle micrographs were obtained using transmission electron microscope (TEM) JEM-2100 (JEOL, Tokyo, Japan) integrated with X-Max energy dispersive spectrometer (EDS) (Oxford Instruments, Abingdon, UK) and scanning electron microscope (SEM) LEO EVO 50 (Carl Zeiss AG, Jena, Germany), equipped with an INCA-Energy 450 EDS analyzer (Oxford Instruments, Abingdon, UK). The phase compositions of the powder were determined using X-ray diffractometer (XRD) Shimadzu XRD-7000 (Shimadzu, Kyoto, Japan), CuKα radiation. The data obtained were processed using XPowder CELL 2.4 ver.2004 software package. Particle size distribution was determined using CPS 24000 Disc Centrifuge (CPS Instruments Inc., Los Angeles, CA, USA).

FTIR spectra of Ti–Al powder, MC2162 polymer binder, as well as the feedstock prepared were recorded on Nikolet 5700 (Thermo Electron, Waltham, MA, USA) spectrophotometer in KBr pellets. The spectra have been measured in the spectral range of 4000–400 cm^{-1}.

The specific surface area of the powders was evaluated by the nitrogen adsorption-desorption method using the Sorbtometer M (Katakon, Russia) apparatus and calculated by the BET method.

2.3. Preparation of the Powder–Polymer Feedstock

Ti–Al powders are indeed prone to oxidation. Therefore, the synthesized powders are stored and processed in an inert atmosphere. For this purpose, Z-blade mixer SPQ-10 (Welber, Hangzhou, China), the single screw extruder LE45-30 (Scientific, Muang, Thailand), the synthesized Ti–Al powder in a tight vessel filled with inert gas, and MC2162 polymer binder (Emery Oleochemicals, Loxstedt, Germany) were placed in a glove box. The MC2162 binder is a mixture of polyol ester and polyamide. Next, the air was evacuated from the glove box and then it was filled with argon. The powder and binder in a ratio of 60:40 vol.% were mixed in a Z-blade mixer SPQ-10 with a 60 rpm rotational speed and a mixing time of 6 h. The mixture was then transferred to the single screw extruder LE45-30 and extruded at 145 °C to produce powder–polymer feedstock.

Melt flow index (MFI) of the powder–polymer feedstock was measured using plastometer IIRT-M (Himpribor-1, Tula, Russia). The feedstock MFI measurements were carried out with a load of 5 kg (50 N) at 155 °C (ASTM 1238-73). Moreover, the viscosity (ν, Pa·s) of obtained feedstocks was determined by the expression (3) from the MFI value as described by Shenoy et al. [29].

$$\nu = k\frac{\rho}{MFI}, \quad (3)$$

where k—is a constant that depends on the characteristics of the *MFI* measuring device, and is equal to 4257.6 [29], ρ—is a density of the powder–polymer feedstock.

3. Results and Discussion

3.1. Preparation and Characterization of Ti–Al Powders

Ti–Al particles were obtained by the EEW of the titanium and aluminum wires in an argon medium. In the EEW process, the high current pulse passes through the wires giving the metal vapors and droplets. Interaction of these species in gas medium followed by rapid cooling results in the formation of both Ti–Al nanoparticles and microparticles.

Figure 1 shows an oscillogram curves of the current $I(t)$ passing through the wires and the energy values $E(t)$ introduced into the wires. It follows from the curves in Figure 1 that as U_0 grows, the current density (1.2×10^7 A/cm^2 $\leq j \leq 1.8 \times 10^7$ A/cm^2) and the rate of energy input into the wire increase. The energy input time falls from 2.6 μs to 2 μs, which contributes to a decrease in the width of the particle size distribution in powders obtained by EEW method [26].

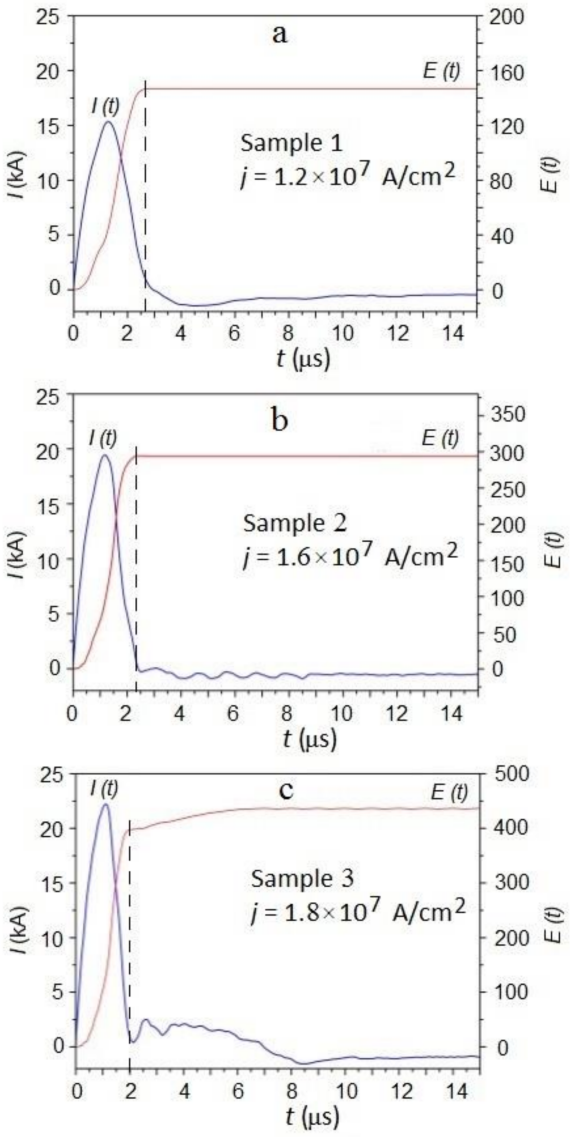

Figure 1. Oscillogram curves of the current $I(t)$ passing through the wires and the energy $E(t)$ introduced into the wires for samples from Table 1: (**a**) sample 1; (**b**) sample 2; (**c**)—sample 3.

Analysis of the particle size distribution (Figure 2) showed that at a minimum energy introduced into the wire being 147 J (Sample 1), both nanoparticles and microparticles are formed. The size distribution curve displays two maxima (bimodal powder), the first of

which is in the region of nanosizes (59 nm), and the second, in the region of micron (2 μm) sizes (Table 2). The energies being 292 J and 430 J (Sample 2 and 3), the size distribution curves display one maximum (monomodal distribution) at 132 and 95 nm, respectively. As the energy *E* transferred to the wires increases, the maximum of the distribution functions shifts to a region of smaller sizes.

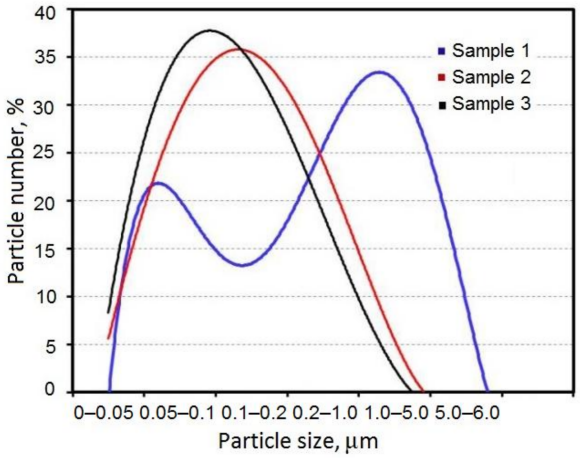

Figure 2. Size distribution of Ti–Al particles.

Table 2. Specific surface area and particle size distribution maximum versus EEW parameters.

Sample	$I(t)$ 10^7 (A/cm^2)	E (J)	$E(t)/t$ (J/μs)	Specific Surface Area (m^2/g)	Size Distribution Maximum
1	1.2	147	56.5	9.4	59 nm, 2 μm
2	1.6	292	127	10.5	132 nm
3	1.8	430	215	11.5	95 nm

The specific surface area of powders obtained at different values of the energy introduced into the wires increases with an increase in the explosion energy of the wires (Table 2). This also indicates that an increase in the value of *E* leads to an increase in the number of small particles.

It follows from the TEM images of powders obtained (Figure 3) that for the Sample 1 which was obtained at the minimum energy introduced, along with nanoparticles with a size of less than 100 nm and microparticles with a size of more than 1 μm, submicron particles with a size from 0.1 to 1 μm are observed.

Typical images of Ti–Al composite particles and elemental analysis using EDS mapping are shown in Figures 4–6. It follows from the powder images and analysis data that the samples consist of microparticles, submicron, and nanoparticles, and Al and Ti are homogeneously distributed in Ti–Al particles. It should be noted that particles larger than 100 nm are present in all samples.

The initial titanium content in the two twisted wires is 72.3 wt.%, aluminum—27.7 wt.%. However, in accordance with the data presented in Figures 4–6, the aluminum content in the powders is somewhat higher and titanium is less than in the wire twist. The titanium content in the powders increases from 61 wt.% up to 66.5 wt.% as the energy introduced into the wire increases. At the same time, a number of titanium particles were found welded to the walls of the Reactor setup. Since the particle size decreases with the increase of E value, it can be assumed that, in general, some part of the large particles is welded to the walls. The presence of individual large particles (more than 20 μm) of titanium in the samples is due to the features of the EEW process. Since the electrical resistivity of titanium significantly exceeds the electrical resistivity of aluminum, the energy introduced into the titanium wire is less than

that introduced into the aluminum wire [26]. Due to the difference in the energies introduced into the wires, the expanding products of the simultaneous EEW when exploding titanium and aluminum wires are a homogeneous mixture, which, by mass, consists mainly of submicron and micron titanium particles and nanosized aluminum clusters. In this case, the mass fraction of titanium in the powder, which is captured by filter F, decreases.

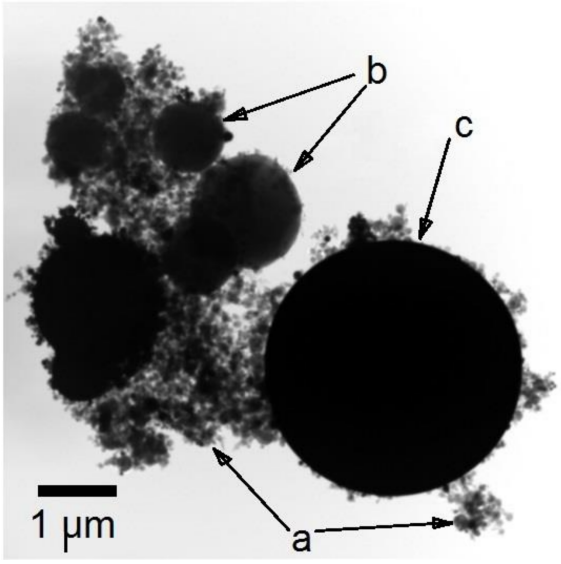

Figure 3. TEM images of the particles obtained at $E(t)$ = 147 J (Sample 1): a—nanoparticles, b—submicron particles, c—microparticles.

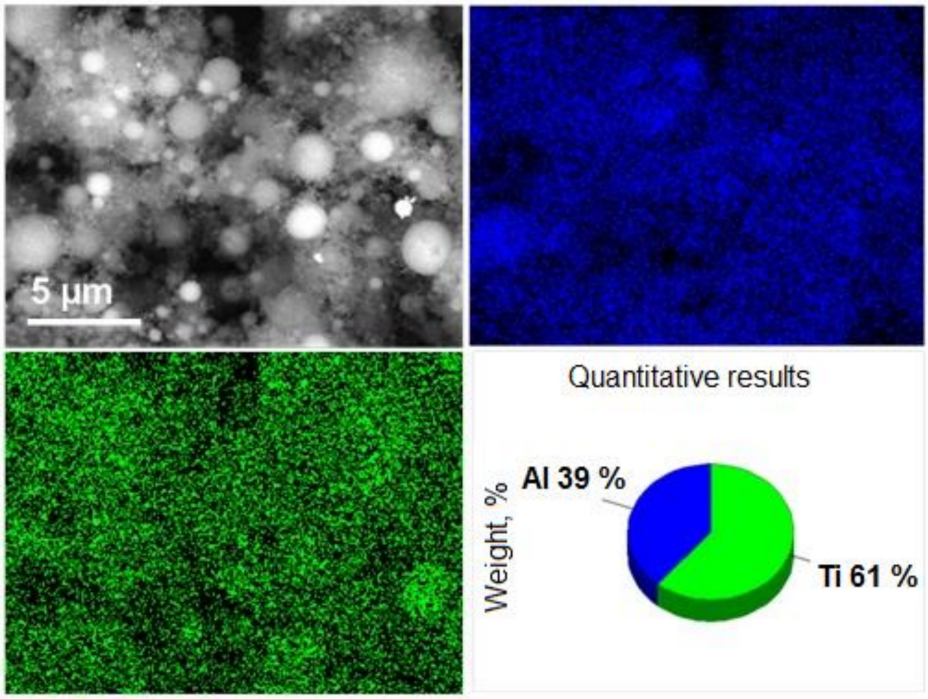

Figure 4. TEM images of the Ti–Al particles, element distribution and metal ratio in Sample 1.

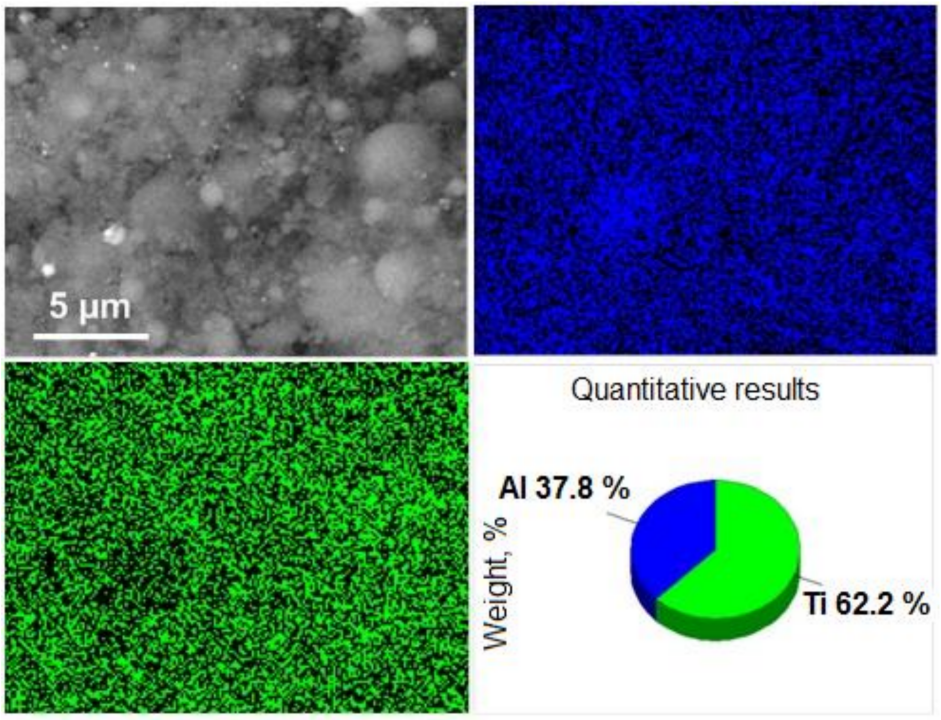

Figure 5. TEM images of the Ti–Al particles, element distribution and metal ratio in Sample 2.

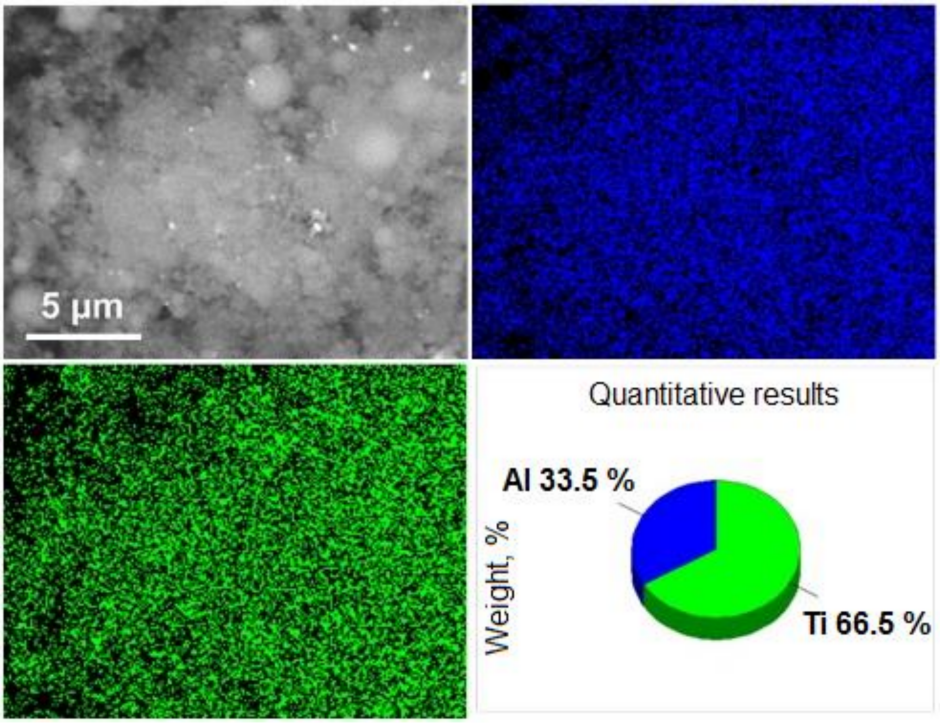

Figure 6. TEM images of the Ti–Al particles, element distribution and metal ratio in Sample 3.

Figure 7 shows the XRD patterns of the Ti–Al powders obtained. The diffraction peaks indicate that the samples contain both intermetallic phases (TiAl, Ti_3Al) and pure aluminum and titanium phases. As the energy introduced increases from E = 147 J (Sample 1) to E = 430 J (Sample 3), the content of TiAl and Ti_3Al in the samples increases. In this case, the aluminum content in the wire dispersion products is 40.5 at.%, the titanium content is

59.5 at.%. In accordance with the aluminum–titanium phase diagram [30], α-Ti in alloys with a high aluminum content (39–46.5 at.%) decomposes into a mixture of Ti_3Al and TiAl. Probably, the metal melt is initially formed during the passage of high-power current pulse in the aluminum and titanium wires, with the content of components corresponding to that in the wires. On cooling the melt, Ti_3Al and TiAl phases are formed.

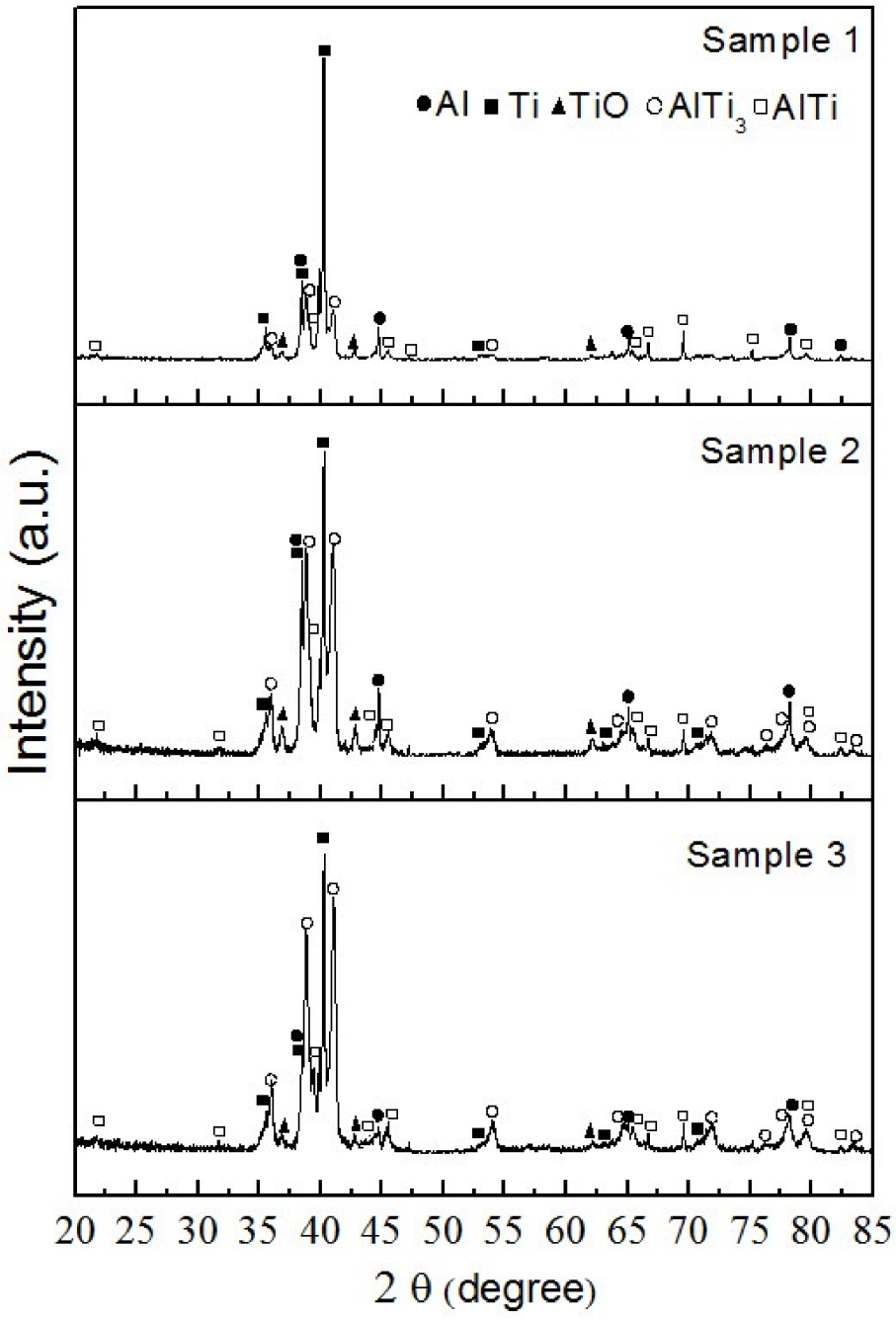

Figure 7. XRD patterns of Ti–Al powders.

Element distribution in the particles of Sample 1 showed that nanoparticles and submicron particles include both titanium and aluminum (Figure 8a,b). In addition, there are particles larger than 10 μm in size, mainly consisting of either aluminum (Figure 8c) or titanium (Figure 8d). With an increase in the energy introduced into the wires (E = 292 J

for Sample 2 and E = 430 J for Sample 3) the same is observed, that is, both titanium and aluminum are uniformly distributed in nanoparticles and submicron particles.

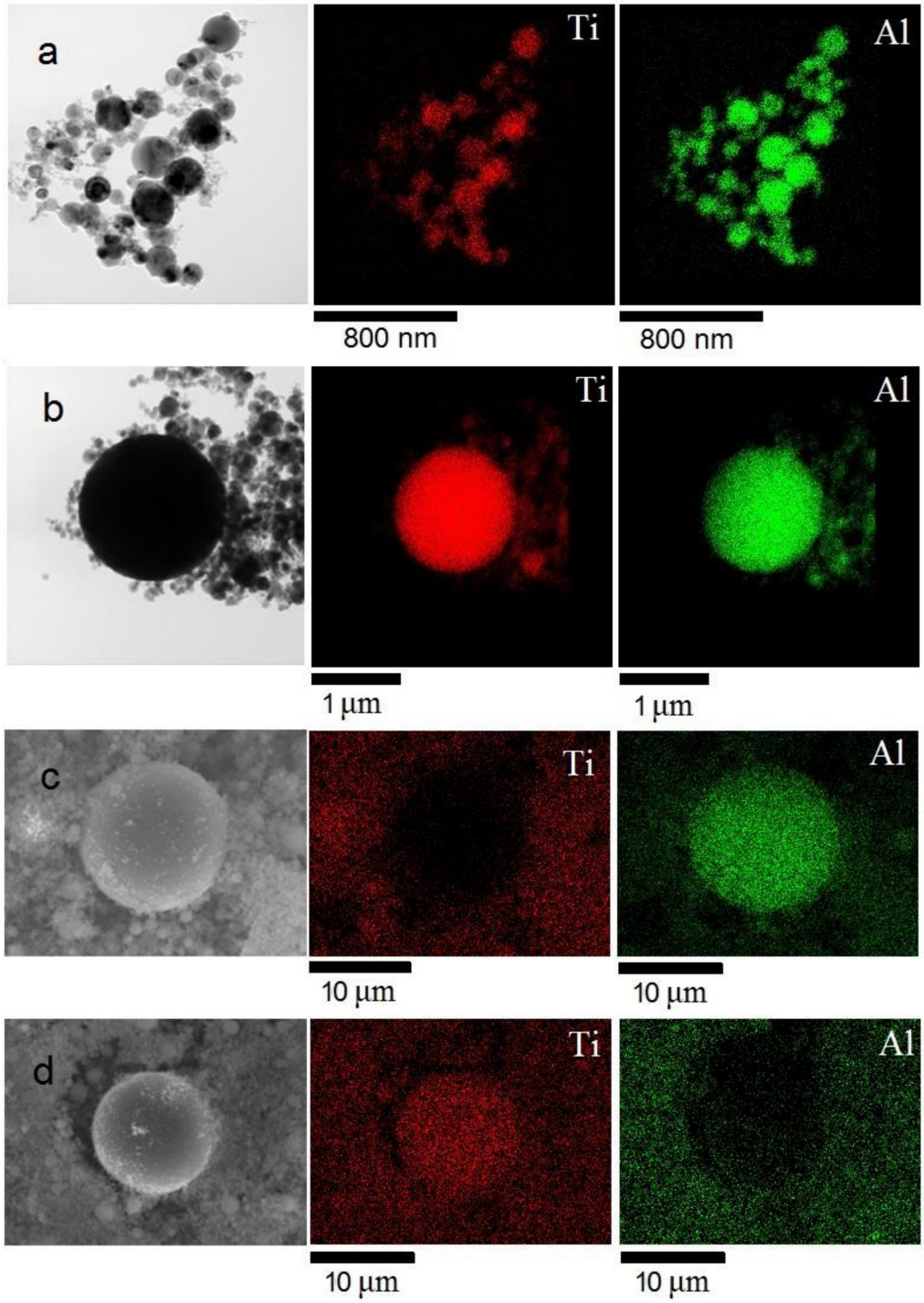

Figure 8. Titanium and aluminum distribution in particles (Sample 1): (**a**) nanoparticles, (**b**) submicron particles, (**c**,**d**) microparticles.

The formation of bimetallic nanoparticles was reported to occur due to the assembling of metal clusters formed at the initial stages of the exploding process of two wires of dissimilar metals [31]. Moreover, with an increase in the energy introduced into the wires, the number of nanoparticles increases [24].

Similarly, the formation of Ti–Al nanoparticles and submicron particles occurs when metal clusters assembly. Hence it follows that with increasing energy introduced into the wires, the fraction of nanoparticles containing intermetallides will increase. At low values of the energy introduced into the wires, the content of nanoparticles will be lower, and a significant fraction of the powder will consist of titanium and aluminum microparticles [27]. The particle size distribution curves (Figure 1) confirm that at E = 147 J the mechanism of particle formation is different. This leads to the fact that a significant number of microparticles are formed through liquid-drop disintegration of the wire metal. Such microparticles (Figure 8c,d) consist of either aluminum or titanium.

3.2. The Powder–Polymer Feedstock Characterization

The Ti–Al powders obtained were used to prepare powder–polymer feedstocks. The 60 vol.% loading with the powder ensured the feedstock homogeneity and provided high flowability of the feedstock. Powder–polymer feedstock prepared from Sample 1 of Ti–Al powder was designated as bimodal feedstock 1, respectively, the feedstocks 2 and 3 prepared from Sample 2 and Sample 3 of Ti–Al powders were designated as monomodal ones.

The SEM images in Figure 9 show the fracture surface of the powder–polymer feedstocks 1–3. Study of the SEM images of fracture surfaces showed that microparticles, submicron and nanoparticles in both bimodal feedstock 1 and monomodal feedstocks 2 and 3 are evenly distributed. Moreover, the number of microparticles in the bimodal feedstock 1 is higher compared to the monomodal feedstocks 2 and 3. In addition, no pores are visible in the cross-section of the bimodal feedstock 1 as well as in monomodal feedstocks 2 and 3. This indicates that the all feedstocks were of good quality.

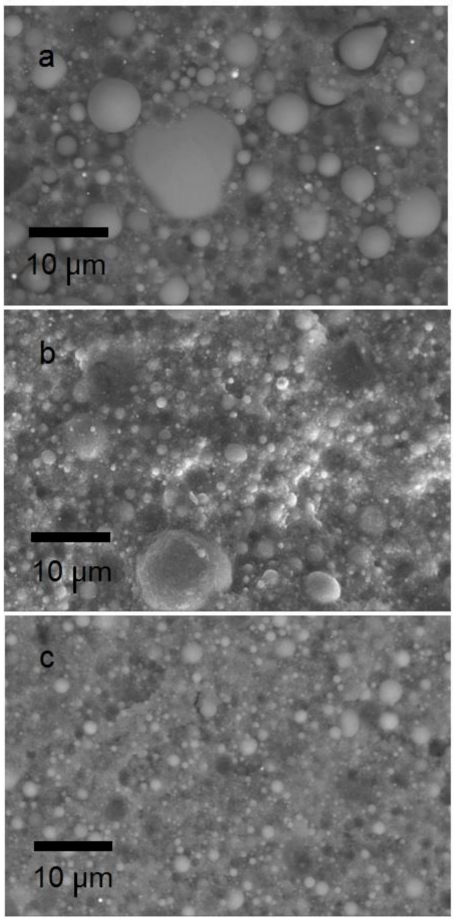

Figure 9. SEM images of the powder–polymer feedstock fracture surfaces: (**a**) feedstock 1, (**b**) feedstock 2, (**c**) feedstock 3.

The results of measuring the bimodal and monomodal feedstock melt flow indices are presented in Table 3. The bimodal feedstock 1 containing a larger number of microparticles has a higher flowability (MFI = 310 ± 10 g/10 min) compared to the monomodal feedstocks 2 and 3 (230 ± 10 g/10 min and 170 ± 10 g/10 min, respectively), where the content of nanoparticles is higher.

Table 3. Feedstock melt flow indices and viscosity.

Sample	MFI (g/10 min)	ν (Pa·s)
bimodal feedstock 1	310 ± 14	41.4 ± 0.6
monomodal feedstock 2	230 ± 16	55.9 ± 0.6
monomodal feedstock 3	170 ± 19	75.6 ± 0.6

Ti–Al powders are prone to oxidation. Therefore, the synthesized powders are stored and processed in an inert atmosphere. FTIR spectra were used to determine the presence of titanium and aluminum oxides in the powder–polymer feedstock. Figure 10 shows comparative FTIR spectra of Ti–Al powder (sample 1) stored in air (red line), MC2162 polymer binder (pink line) and bimodal feedstock 1 (black line).

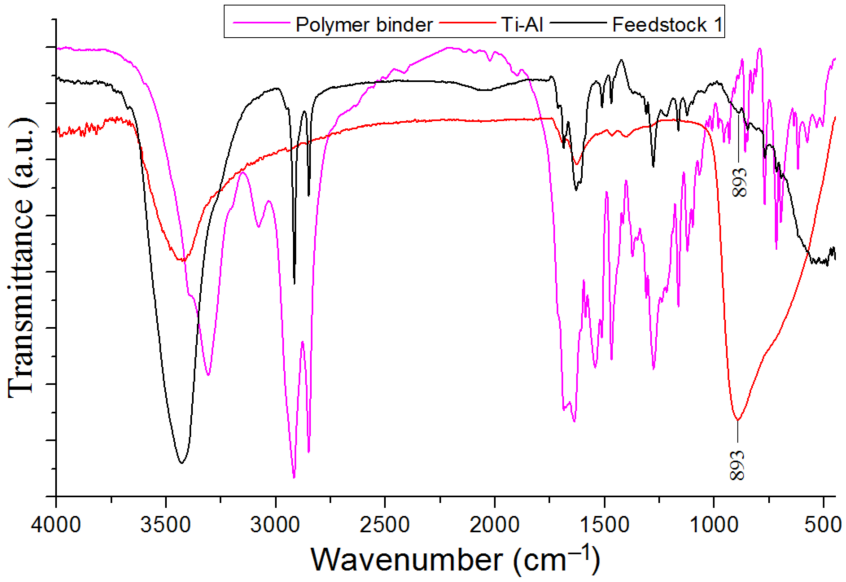

Figure 10. FTIR spectra of Ti–Al powder (sample 1) stored in air (red line), MC2162 polymer binder (pink line) and bimodal feedstock 1 (black line).

Stretching vibrations of Al-O and Ti-O bands appear in the IR spectrum of Ti–Al powder (red line) as a wide absorption band in the region of 950 . . . 500 cm^{-1} having several maxima. At the same time, there is only a weak band at 893 cm^{-1} in the IR spectrum of bimodal feedstock 1 (black line). This indicates the significant oxidation of the powder stored in air. Whereas for the bimodal feedstock 1 prepared in an inert medium, no significant oxidation of Ti–Al powder occurs.

The positive effect of using bimodal powders obtained by mixing micro- and nanoparticles when preparing the bimodal feedstocks has also been shown by many authors [8,10,17,19,22,32–34] and in our recent study [28,35]. Meanwhile, an increase in the bimodal feedstock viscosity with an increase in the content of nanoparticles above the optimal value was noted by Oh J.W. et al. [36–38]. A similar trend is observed for bimodal feedstock based on bimodal powders produced by EEW method (Table 3). Thus, for AM technology the advanced feedstock performance can be provided by the optimal bimodal size distribution of the powder filler [39]. So, the use of a bimodal powder

can be concluded to effectively reduce the bimodal feedstock viscosity while maintaining a uniform distribution of micro- and nanoparticles.

4. Conclusions

The simultaneous electrical explosion of titanium and aluminum wires was used to produce Ti–Al powders. The destruction of the wire material under the action of a high current pulse yields both liquid metal droplets and metal vapor, giving nano-, submicro- and microparticles upon cooling.

The level of energy introduced into Ti and Al wires has been found to determine the form of the particle size distribution function, specific surface area, and phase composition of particles in powders obtained by EEW method. The bimodal distribution of particles in powders obtained is achieved at a current density of 1.2×10^7 A/cm^2 (the rate of energy input is 56.5 J/μs). In this case, the synthesized nanoparticles and submicron particles consist of Ti_3Al and TiAl alloys, while presenting microparticles which consist of titanium or aluminum. As the energy introduced into the wires increases, the maximum of the particle distribution function shifts towards smaller sizes, turning into a monomodal distribution, while the content of intermetallic phases in the samples increases.

For the powder–polymer feedstocks prepared with Ti–Al powders, a tendency to increase in MFI with an increase in the number of microparticles is observed. The bimodal feedstock prepared with bimodal powders had a higher MFI than monomodal feedstocks with a predominance of nanoparticles. In addition, a homogeneous distribution of microparticles, submicron, and nanoparticles in all feedstocks was observed.

The presented study, using the example of Ti–Al powders, describes a new approach for the synthesis of bimodal powders of complex phase composition with a homogeneous distribution of micro- and nanoparticles by the electrical explosion of the twisted wires of dissimilar metals. This approach can be used for the industrial production of bimodal powders for powder–polymer feedstocks with a high melt flow index value.

Author Contributions: Conceptualization, M.L. and E.G.; methodology, A.P. and E.G.; validation, A.P. and O.B.; investigation, K.S., S.K., N.T. and O.B.; writing—original draft preparation, M.L. and N.R.; writing—review and editing, E.G. and N.R.; visualization, S.K. and N.T. All authors have read and agreed to the published version of the manuscript.

Funding: The study was supported by a grant from the Russian Science Foundation (project No. 21-79-30006).

Institutional Review Board Statement: Not applicable.

Informed Consent Statement: Not applicable.

Data Availability Statement: Data sharing is not applicable.

Conflicts of Interest: The authors declare no conflict of interest.

References

1. Hegab, H.A. Design for additive manufacturing of composite materials and potential alloys: A review. *Manuf. Rev.* **2016**, *3*, 11–17. [CrossRef]
2. Gill, S.S.; Kaplas, M. Comparative Study of 3D Printing Technologies for Rapid Casting of Aluminium Alloy. *Mater. Manuf. Process.* **2009**, *24*, 1405–1411. [CrossRef]
3. Kristiawan, R.B.; Imaduddin, F.; Ariawan, D.; Ubaidillah; Arifin, Z. A review on the fused deposition modeling (FDM) 3D printing: Filament processing, materials, and printing parameters. *Open Eng.* **2021**, *11*, 639–649. [CrossRef]
4. Zhang, J.; Amini, N.; Morton, D.A.; Hapgood, K.P. 3D printing with particles as feedstock materials. *Adv. Powder Technol.* **2021**, *32*, 3324–3345. [CrossRef]
5. Gonzalez-Gutierrez, J.; Cano, S.; Schuschnigg, S.; Kukla, C.; Sapkota, J.; Holzer, C. Additive Manufacturing of Metallic and Ceramic Components by the Material Extrusion of Highly-Filled Polymers: A Review and Future Perspectives. *Materials* **2018**, *11*, 840. [CrossRef] [PubMed]
6. Subaşı, M.; Safarian, A.; Karataş, Ç. An investigation on characteristics and rheological behaviour of titanium injection moulding feedstocks with thermoplastic-based binders. *Powder Met.* **2019**, *62*, 229–239. [CrossRef]

7. Giberti, H.; Strano, M.; Annoni, M. An innovative machine for Fused Deposition Modeling of metals and advanced ceramics. In *Proceedings of the MATEC Web of Conferences*; EDP Sciences: New York, NY, USA, 2016; Volume 43, p. 3003.
8. Choi, J.-P.; Lyu, H.-G.; Lee, W.-S.; Lee, J.-S. Investigation of the rheological behavior of 316L stainless steel micro-nano powder feedstock for micro powder injection molding. *Powder Technol.* **2014**, *261*, 201–209. [CrossRef]
9. Bricout, J.; Gelin, J.-C.; Ablitzer, C.; Matheron, P.; Brothier, M. Influence of powder characteristics on the behaviour of PIM feedstock. *Chem. Eng. Res. Des.* **2013**, *91*, 2484–2490. [CrossRef]
10. Oh, J.W.; Ryu, S.K.; Lee, W.S.; Park, S.J. Analysis of compaction and sintering behavior of 316L stainless steel nano/micro bimodal powder. *Powder Technol.* **2017**, *322*, 1–8. [CrossRef]
11. Suri, P.; Atre, S.V.; German, R.M.; de Souza, J.P. Effect of mixing on the rheology and particle characteristics of tungsten-based powder injection molding feedstock. *Mater. Sci. Eng. A* **2003**, *356*, 337–344. [CrossRef]
12. Li, J.; Pan, Y.; Qiu, F.; Huang, L.; Guo, J. Alumina ceramics fabricated from bimodal alumina with additives. *Mater. Sci. Eng. A* **2006**, *435–436*, 611–619. [CrossRef]
13. Prabhu, T.R. Effect of bimodal size particles reinforcement on the wear, friction and mechanical properties of brake composites. *Tribol. Mater. Surf. Interfaces* **2016**, *10*, 163–171. [CrossRef]
14. Rajabi, J.; Muhamad, N.; Sulong, A.B.; Fayyaz, A.; Raza, M.R. The effect of nano-sized stainless steel powder addition on mechanical and physical properties of micropowder injection molded part. *Mater. Des.* **2014**, *63*, 223–232. [CrossRef]
15. Crane, N.B.; Wilkes, J.; Sachs, E.; Allen, S.M. Improving accuracy of powder-based SFF processes by metal deposition from a nanoparticle dispersion. *Rapid Prototyp. J.* **2006**, *12*, 266–274. [CrossRef]
16. Du, W.; Singh, M.; Singh, D. Binder jetting additive manufacturing of silicon carbide ceramics: Development of bimodal powder feedstocks by modeling and experimental methods. *Ceram. Int.* **2020**, *46*, 19701–19707. [CrossRef]
17. Rajabi, J.; Fayyaz, A. Effects of Nanopowder Addition on Rheological Properties of Feedstock for Micropowder Injection Moulding Process. *J. Kejuruteraan.* **2019**, *31*, 229–241. [CrossRef]
18. Pervikov, A.; Rodkevich, N.; Glazkova, E.; Lerner, M. Bimodal metal micro-nanopowders for powder injection molding. *AIP Conf. Proc.* **2017**, *1915*, 040045. [CrossRef]
19. Oh, J.W.; Seong, Y.; Shin, D.S.; Park, S.J. Investigation and two-stage modeling of sintering behavior of nano/micro-bimodal powders. *Powder Technol.* **2019**, *352*, 42–52. [CrossRef]
20. Bai, Y.; Wagner, G.; Williams, C.B. Effect of Particle Size Distribution on Powder Packing and Sintering in Binder Jetting Additive Manufacturing of Metals. *J. Manuf. Sci. Eng.* **2017**, *139*, 081019. [CrossRef]
21. Song, J.-L.; Lee, G.-Y.; Hong, E.-J.; Lee, C.S.; Lee, J.-S. Sintering behavior of bimodal iron nanopowder agglomerates. *J. Am. Ceram. Soc.* **2019**, *102*, 3791–3801. [CrossRef]
22. Macak, J.; Syrovy, T.; Wagner, T.; Kubac, L.; Josefik, F. Method for Preparation of a Bimodal Mixture of Copper Nanoparticles and Microparticles with a Polymeric Protective Layer, a Bimodal Mixture of Copper Nanoparticles and Microparticles with a Polymeric Protective Layer Prepared by This Method and a Printing Formula Containing This Bimodal Mixture. WO Patent No. WO2016045648, 31 March 2016.
23. Kim, K.-H.; Choi, H.; Han, C. Tungsten Micropowder/Copper Nanoparticle Core/Shell-Structured Composite Powder Synthesized by Inductively Coupled Thermal Plasma Process. *Met. Mater. Trans. A* **2017**, *48*, 439–445. [CrossRef]
24. Lerner, M.I.; Svarovskaya, N.V.; Psakhie, S.G.; Bakina, O.V. Production technology, characteristics, and some applications of electric-explosion nanopowders of metals. *Nanotechnol. Russ.* **2009**, *4*, 741–757. [CrossRef]
25. Sedoi, V.S.; Ivanov, Y.F. Particles and crystallites under electrical explosion of wires. *Nanotechnology* **2008**, *19*, 145710. [CrossRef] [PubMed]
26. Pervikov, A.; Glazkova, E.; Lerner, M. Energy characteristics of the electrical explosion of two intertwined wires made of dissimilar metals. *Phys. Plasmas* **2018**, *25*, 070701. [CrossRef]
27. Lerner, M.; Pervikov, A.; Glazkova, E.; Rodkevich, N.; Toropkov, N. Electrical Explosion Synthesis, Oxidation and Sintering Behavior of Ti-Al Intermetallide Powders. *Metals* **2021**, *11*, 760. [CrossRef]
28. Pervikov, A.; Toropkov, N.; Kazantsev, S.; Bakina, O.V.; Glazkova, E.; Lerner, M. Preparation of Nano/Micro Bimodal Aluminum Powder by Electrical Explosion of Wires. *Materials* **2021**, *14*, 6602. [CrossRef]
29. Shenoy, A.V.; Saini, D.R.; Nadkarni, V.M. Melt Rheology of Polymer Blends from Melt Flow Index. *Int. J. Polym. Mater. Polym. Biomater.* **1984**, *10*, 213–235. [CrossRef]
30. Schuster, J.C.; Palm, M. Reassessment of the binary Aluminum-Titanium phase diagram. *J. Phase Equilibria Diffus.* **2006**, *27*, 255–277. [CrossRef]
31. Lerner, M.I.; Pervikov, A.V.; Glazkova, E.A.; Svarovskaya, N.V.; Lozhkomoev, A.; Psakhie, S.G. Structures of binary metallic nanoparticles produced by electrical explosion of two wires from immiscible elements. *Powder Technol.* **2016**, *288*, 371–378. [CrossRef]
32. Choi, J.-P.; Park, J.-S.; Hong, E.-J.; Lee, W.-S.; Lee, J.-S. Analysis of the rheological behavior of Fe trimodal micro-nano powder feedstock in micro powder injection molding. *Powder Technol.* **2017**, *319*, 253–260. [CrossRef]
33. You, W.-K.; Choi, J.-P.; Yoon, S.-M.; Lee, J.-S. Low temperature powder injection molding of iron micro-nano powder mixture. *Powder Technol.* **2012**, *228*, 199–205. [CrossRef]
34. Oh, J.W.; Bollina, R.; Lee, W.S.; Park, S.J. Effect of nanopowder ratio in bimodal powder mixture on powder injection molding. *Powder Technol.* **2016**, *302*, 168–176. [CrossRef]

35. Krinitcyn, M.; Toropkov, N.; Pervikov, A.; Glazkova, E.; Lerner, M. Characterization of nano/micro bimodal 316L SS powder obtained by electrical explosion of wire for feedstock application in powder injection molding. *Powder Technol.* **2021**, *394*, 225–233. [CrossRef]
36. Oh, J.W.; Seong, Y.; Park, S.J. Effect of nanoparticles in bimodal powder on physical and mechanical properties of powder injection molded parts. *J. Mater. Process. Technol.* **2018**, *262*, 503–510. [CrossRef]
37. Oh, J.W.; Park, J.M.; Shin, D.S.; Noh, J.; Park, S.J. Comparative study of nanoparticle effects on feedstock behavior for injection molding. *Mater. Manuf. Process.* **2019**, *34*, 414–421. [CrossRef]
38. Oh, J.W.; Lee, W.S.; Park, S.J. Nanopowder Effect on Fe Nano/Micro-Bimodal Powder Injection Molding. *Met. Mater. Trans. A* **2018**, *49*, 5535–5545. [CrossRef]
39. Rueda, M.M.; Auscher, M.-C.; Fulchiron, R.; Périé, T.; Martin, G.; Sonntag, P.; Cassagnau, P. Rheology and applications of highly filled polymers: A review of current understanding. *Prog. Polym. Sci.* **2017**, *66*, 22–53. [CrossRef]